

## **Developing a Magnetogenetic Sensor for Non-Invasive Activation Pathways**

Michael Becich, Thomas Lau, Sreyas Misra  
December 6th, 2015

## Abstract

As the discipline of synthetic biology continues to expand, tools for targeted manipulation of gene regulation are increasingly relevant and applicable. Light-activated systems have led to major breakthroughs in optogenetics for neuromodulation; however, a major limitation is light's ability to permeate tissue, requiring invasive methods to deliver light which has halted medical applications. Inspired by recent breakthroughs (Long et al. 2015), we present a system for HEK293T cells using a iron-sulfur cluster assembly homologue (IscA1) from *columba livia*, codon-optimized for *homo sapiens*, to sense the presence of a magnetic field and activate a GFP-fusion (Green Fluorescent Protein) construct (GCaMP6s, which activates modular GFP expression in the presence of calcium (*DNA 2.0, Menlo Park, CA, U.S.A.*)). In our pilot study, after transient co-transfection of the IscA and GCaMP6s plasmids, we measured fluorescent readout over time upon exposure to various 0-1mT magnetic fields. Our results reveal strong binary (on/off) control at B-field levels in the presence of any magnetic field ( $p=0.0009$  for 0mT vs 1mT trials); a statistically significant difference in fluorescent expression is thresholded at values above 0.25mT for IscA1-based constructs (no significant fluorescence change was observed for IscA2 at any magnetic field strength). However, precise modular control of fluorescent expression with varied magnetic strength was not observed due to our small sample size in a constrained setting ( $R=0.87$  for IscA1 fluorescent expression vs. magnetic field strength). Nonetheless, our IscA-based magnetogenetic system opens the door for future refinements and applications in noninvasive neuromodulation, CRISPR-Cas9 delivery, and targeted gene therapy.

## Introduction

Neuromodulation methods such as optogenetics have allowed scientists to explore the inner-workings of complicated neural networks *in vivo*.<sup>1</sup> Understanding how neural networks respond to external stimuli has given scientists powerful research tools in synthetic biology. However, while optogenetics has given researchers unprecedented insight into the inner workings of neural networks *in-vivo*, the effects of heat/light and the presence of foreign optogenetic proteins in cells can result in undesirable cellular side effects; convoluting original cellular circuitry and therefore producing neural artifacts in experimental results.<sup>2</sup> The abilities of optogenetics are limited by light's ability to permeate tissue, requiring invasive methods to deliver the light. Thus, there exists an unmet need for an accurate, modular, and noninvasive gene expression sensor system.

On the other hand, recent advances in identifying the cellular mechanisms involved with the magnetic activation of neural pathways, such as magnetoreception in homing pigeons (Fig. 1), have unlocked the potential for magnetogenetic sensors to guide neuromodulation. Magnetogenetic methods, if implementable, are preferable to optogenetic regulation because they are non-invasive, deeply penetrating, long-term continuous dosing, spatially uniform, and safely accessible without unintended consequences.



**Figure 1. Inspiration:** The inspiration of this investigation comes from synthetic biology principles of modelling nature. Species such as the homing pigeon (*columba livia*) navigate via magnetic sensing; however, the biochemical mechanism is not well understood. Many other species like wolves and eagles also possess magnetic sensing capabilities.

Three separate research groups have identified iron-sulfur assembly proteins (IscA) as the mechanism of magnetic sensing in several species (including humans).<sup>3,4,5</sup> This discovery of a native protein with magnetic sensing capabilities lends particular promise to a magnetogenetic system in which the IscA protein complex could serve as sensor to trigger the transcription of cellular/genetic actuators. In September 2015, Long et al. established that activating the IscA magnetoreceptor with a slight external magnetic field causes calcium influx in cells.<sup>6</sup> However, no well-established mechanism by which IscA protein complexes sense magnetic fields or reproducible method for magnetogenetic activation exists.

We constructed two novel magnetic biosensors using the IscA1 and IscA2 protein complexes in HEK293T cells with potential application in neuromodulation. Using these constructs in tandem with a GCaMP6s ultrasensitive calcium influx indicator, our research is the first to quantifiably characterize the time-varying calcium response in magnetoreceptor activation and use IscA1 and IscA2 as magnetoreceptors. Additionally, this magnetoreception mechanism has never been studied specifically in HEK239T cells, which have the research-side advantage of binding to an SV40 enhancer in our IscA plasmids that increase protein production.

## Methods: Design

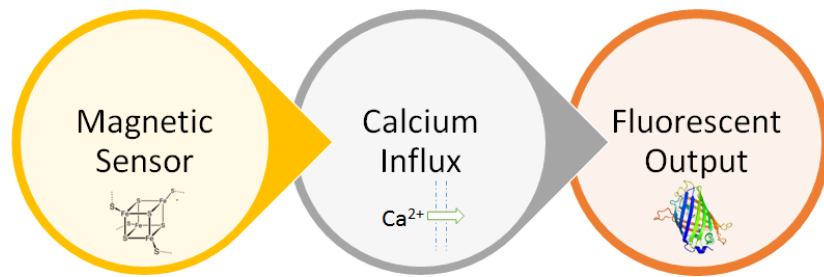


**Figure 2. Abstracted Device Design:** Our sensor device produces a receptor protein (IscA) which depolarizes plasma membranes, triggering calcium influx in the presence of a magnetic field and resulting in fluorescent output

As shown in Figure 2, our device consists of two plasmids that will be co-transfected into mammalian cells. In our prototype, we tested our magnetic receptor as a biological sensor in human embryonic kidney 293T (HEK293T) cells. The first construct constantly transcribes the IscA gene to produce the IscA protein, which acts as a magnetic receptor. It has been theorized “this iron-containing magnetoreceptor might form as an iron-sulfur cluster that could bind to cellular plasma membrane through either cytoskeletons or filaments ... [T]his magnetoreceptor could evoke membrane depolarization and action potentials, generate calcium influx, and trigger neuronal activity in both HEK-293 and cultured primary hippocampal neurons when activated by a remote magnetic field” (Long et al. 2015).<sup>6</sup> After codon-optimizing the amino acid sequence from the pigeon (*columba livia*) for *homo sapiens*, the IscA1 coding sequence was registered on the iGEM Registry of Standard Biological Parts as BBa\_M36907 and the IscA2 coding sequence was registered under BBa\_M36908. More information about modifications we made and the actual sequences can be found at [iGEM Registry](#). Each IscA gene is fused to RudolphRFP by a P2A sequence for easy cleavage to monitor protein expression and confirm translation. In our mammalian cells, antibiotic selection would only be the focus of follow-up projects as we will approximate eukaryotic expression with transient transfections in our pilot study.

The second GCaMP6s construct acts as our indicator and was acquired from Addgene (Plasmid #40753). It is an established slow-kinetics, ultrasensitive protein calcium sensor to detect calcium influx and produce fluorescent output. The GCaMP6s complex is a fusion of a GFP protein and calmodulin (CaM), the latter of which binds to four calcium ions and conformationally changes to activate the GFP. This enables the GCaMP6s protein complex to act as a real-time calcium indicator whereby the presence of calcium induces the complex to fluoresce green light. It is important to note that two different fluorescent signals were chosen as to prevent confusion between the separate signals in the fluorescence assay.

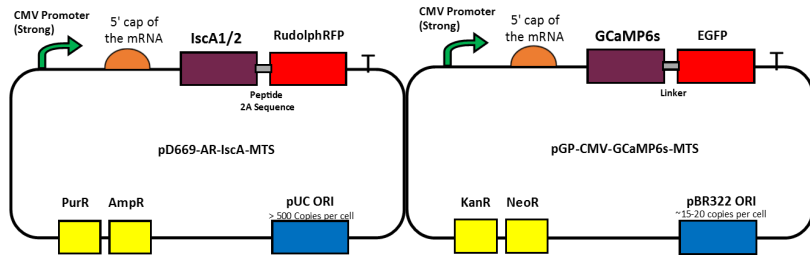


**Figure 3. Sensor constructs:** On the left is the magnetic sensor construct, which translates the IscA gene to Iron-Sulfur protein clusters. On the right, is our GCaMP6s Ultrasensitive Calcium Influx Indicator<sup>8</sup>

## Methods: Experimentation

To create our magnetogenetic system, we first extracted the IscA1, IscA2, and GCaMP6s plasmids from bacterial cells using the standard QIAprep Miniprep procedure. Based on the ThermoFisher Lipofectamine® 3000 Reagent Protocol, we needed 4 µg of IscA1 and IscA2 plasmid, along with 12 µg GCaMP6s. We transformed our plasmids into competent E. coli cells four times (see Practical #3), plating with the appropriate antibiotic (AmpR for IscA1/2 and KanR for GCaMP6s), and culturing overnight for miniprep each time to ensure high concentration yields (measured by Nanodrop Spectrophotometry, see Practical #1). After the GCaMP6s and IscA1/2 plasmids were purified, we co-transfected these plasmids into HEK293T cells, which were passaged every 3 days after initial seeding to have >70% confluence at time of transfection. Due to the time constraints of this project, instead of doing an antibiotic selection, we performed transient transfections and conducted our assays 48-72 hours after transfection when our cells have the highest expression level of our plasmids. Our plasmids are optimized for the transient transfection based on their DNA 2.0 design.

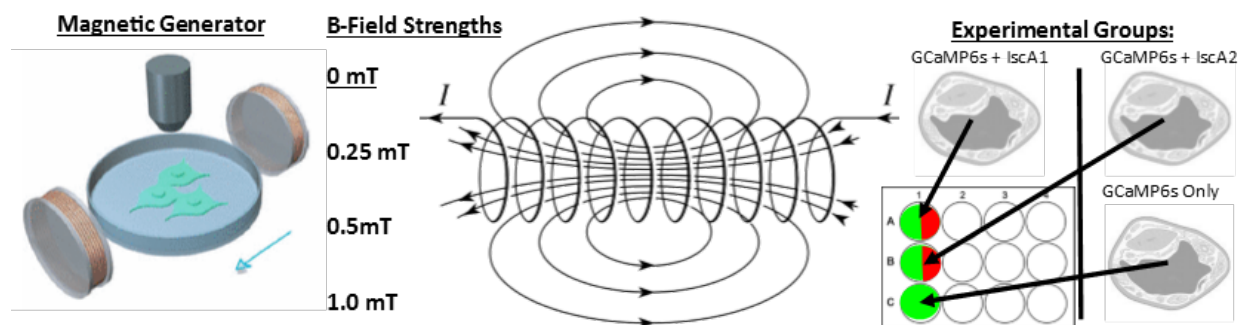


**Figure 4.** We separated our cells into multiple groups of three with each group containing GCaMP6s+IscA1, GCaMP6s+IscA2, and GCaMP6s Only. We subjected each group to different magnetic field strengths. As our positive control, we placed IscA1,2+GCaMP6s in no magnetic field. For our negative control, to account for pleiotropic effects, we placed just GCaMP6s in a magnetic field.

Over the course of three weeks of experimentation, we adjusted our design through two phases of trial and error. 0-1mT is a known magnetic field range established by Long et al.<sup>6</sup> We placed our 12-well plates of cells under a microscope and devised a setup to expose the plates to a magnetic field while reading fluorescence (see Fig. 5). The first was geared towards validating whether our transfections were performed successfully, while the second focused on analyzing the time-response of cells to B-fields.

Phase I: Transfections were performed into 6 12-well plates. Once >70% confluence was achieved, the HEK293T cells were trypsinized for transfection and dilution (see Practical #3, Part 2A). Transfection protocol (per reaction): 1mL DMEM/FBS growth media, 2x50 $\mu$ L Opti-Mem, 500ng of each plasmid, 2 $\mu$ L P3000, 3 $\mu$ L Lipofectamine 3000. Each plate has 3 wells filled (1 IscA1+GCaMP6s, 1 IscA2+GCaMP6s, 1 GCaMP6s only) for a separate magnetic field assay. The plasmids were co-transfected transiently and output was measured **72 hours** after. We used **magnetite** (acquired from Dr. Shih) and the Kinetics Sensor Pro iPhone application to calibrate magnetic field strengths of 0, 0.2, 0.4, 0.6, 0.8, 1.0 mT at corresponding distances [>12, 3, 2.125, 1.625, 1.375, 1.125 in.] such that each plate received a different magnetic field while being imaged. Using our experimental setup described in Fig. 5, we took **still images**, exemplified in Fig. 6, at 20 second intervals in a given location for 2 minutes after exposure for further analysis.

Takeaways: Early signs of fluorescent activation in the IscA1 sensor were apparent, but without refined quantitative analysis, these still image-based results seemed inconclusive. Moreover, we could not compare fluorescence between plates, because the intercellular variance in basal fluorescence proved much larger than variance due to different B-fields. Thus, our second assay in Phase II would have to involve automated time-lapse information to account for basal calcium influx levels. Because our data collection had a sample size of n=1 for each magnetic level, we used time-lapse imaging to take not only multiple images of the same site over 120 seconds (allowing us to express fluorescence as a function of time) but also videos of three sites per field strength (n=3).

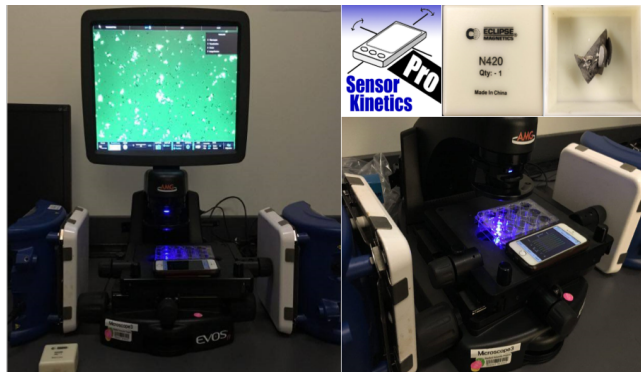


**Figure 5. Experimental Setup:** Our setup consisted of a time-lapse fluorescence microscope, taking images of our sample (shown to be reflecting blue light). The type of fluorescence being measured could be modified by switching from RFP-mode to GFP-mode. Varying the distances between magnetic plate stirrers generated B-fields of varying strength. Because the bulky stir could be placed within a limited range of the sample, we also used small magnetite rocks (top right) to achieve higher field strengths.

The presence of both RFP and GFP confirms that both plasmids were transfected and a magnetic sensing mechanism was underway. But because of “leaky” calcium results and disruptions from human error and image “bleaching” (diminishing of signal), we had to readjust our plan for Phase II.

Phase II: Six different plates for transfection are not necessary, since cells can be reused after removing from a magnetic field. This time, two 12-well plates were used with 3 filled wells (1 IscA1+GCaMP6s, 1 IscA2+GCaMP6s, 1 GCaMP6s only). The same transfection reaction amounts were used but 50 $\mu$ L extra growth media and twice as much DNA was used in an experimental plate since cells showed signs of death after 72 hours in Phase I. The plasmids were transiently co-transfected and assayed **48 hours** after. We calibrated a **magnetic stirrer** (acquired from Dr. Shih) with the Kinetics Sensor Pro iPhone application to magnetic field strengths of 0, 0.25, 0.5, 1.0 mT (corresponded most precisely to stirrer’s modular levels). We took **timelapse images** at 10-second intervals at a given location for 2 minutes after exposure. We then analyzed these time-lapses afterwards, yielding the following results.

Takeaways: Significant (apparent to eye) fluorescence increase in the presence of a magnetic field. Only IscA1 worked. IscA2 showed too discordant signs. The control alone (just GCaMP6s) did not change levels as expected. We could not deduce a modular correlation with our limited sample size however.

Experimental and Control Organization: To understand the integrity of our sensor, we use a null-magnetic-field control to check for the false-positive case where calcium influx is incorrectly triggered even in the absence of a strong magnetic field and the false-negative case where the calcium influx is not triggered in the presence of a strong magnetic field. Before any magnetic field is applied, we measure the RudolphRFP fluorescent output ( $\text{Ex}/\text{Em} = 553/570\text{nm}$ ) to check if the IscA magnetoreceptors are being properly synthesized in the first place as a normalized baseline. We then measure the green fluorescent (EGFP is the variant used in GCaMP6s) output of the cells with a microscope ( $\text{Ex}/\text{Em} = 488/509\text{nm}$ ) to quantify the fluorescent output ratio in order to analyze the temporal response of each of our magnetic sensors. Varying the magnetic field helps us understand the sensitivity of each of our magnetic sensors we have designed with the IscA1 and IscA2 proteins.

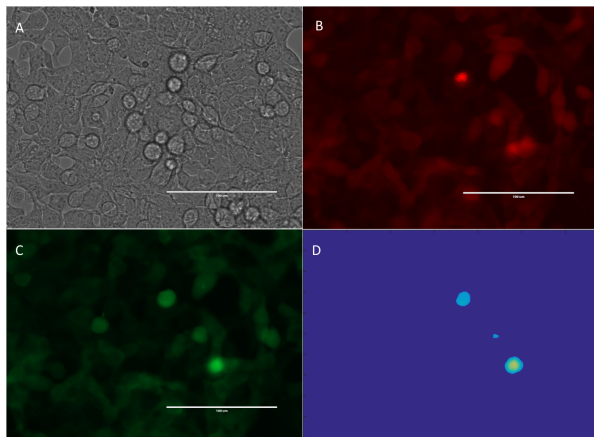
## Results: Image Postprocessing

Image analysis code was written on MATLAB (see Appendix II/III) to postprocess the microscopy images and analyze them for changes in fluorescence over time. The 0.1 frames-per-second (fps) time-lapse videos were separated into individual frames with a 10 second separation. Each frame was individually postprocessed.

First, a 3-sigma gaussian filter was applied to reduce noise. Gaussian filters have the unique advantage over mean filters because the filter can be varied in width and sigma to modulate the range of spatial frequencies present in the image after processing (3-sigma). Moreover, gaussian filters synergize well with canny-edge detection, which we used to calculate the average cell radius.

Second, we employed Otsu's threshold method to remove image artifacts and non-fluorescing objects from the image. Otsu's method divides the image into background regions and object regions. By taking the weighted average between the background versus object pixel intensity values, we could calculate a threshold for each frame; whereby, pixels below the threshold would be floored to 0. Examples of pre-processed and post-processed images can be found in Appendix IV.

Finally, two separate analyses for each time-lapse video were performed. First, normalized fluorescence values for the entire post-processed image were calculated as a function of time (frame-number multiplied by 10 seconds). Using the entire image would provide us fluorescence data for a larger sample of cells. Second, we took the brightest cell in each video and calculated changes in fluorescence over time for just that cell. The location of each cell was recalculated with each frame as to account for movement by cells in the x-y plane due to natural vibrations in the microscope-magnet apparatus. One major source of error, however, occurs with z-axis movement in cells, causing cells' apparent radii to fluctuate. To account for this, we manually subtracted frames where the cell radius changed significantly. A single-cell analysis focuses on our "best data-point," the most brightly fluorescing cell in each video, and calculates fluorescence. All fluorescence values were divided by the number of fluorescing pixels to calculate average pixel fluorescence.



**Figure 6. Still Microscopy Images:** We obtained still microscopy images of all our cells. Cells with IscA1 or IscA2 demonstrated both RFP (B) and GFP (C) fluorescence, implying the successful transfection of both plasmids. GCaMP6s-only cells possessed just GFP fluorescence, because they contained no IscA-1,2 DNA. Image A is a normal image of our co-transfected cells. Image D is a post-processed image of our fluorescent cells, from which we made our calculations.

## Results: Data Analysis

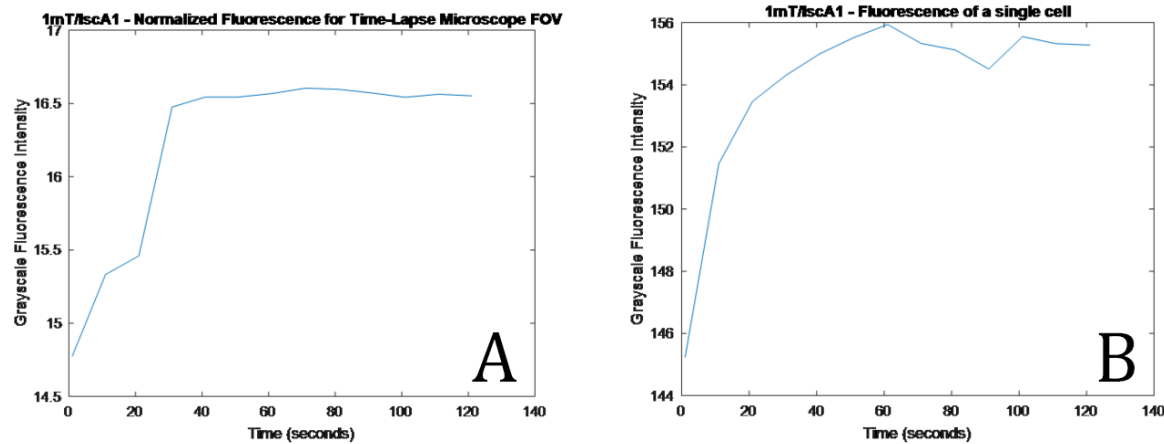


**Figure 7. Preliminary Plots:** Whole Frame (A) and Single Cell (B) vs. time plots were generated by MATLAB

Qualitatively, we observed that B-fields increased cell GFP fluorescence and that fluorescence reached a steady state level after 60 seconds. Subsequent removal of the magnet resulted in an immediate drop of fluorescence values, which returned back to basal levels after  $t_{\infty}=5$  minutes.

After plots (Fig. 7) were generated for each time-lapse video/still-image composite, numerical results were aggregated for analysis. Each two-minute observation was categorized by transfection plasmids (IscA1+GCaMP6s, IscA2+GCaMP6s, GCaMP6s only) and magnetic field strength. The raw GFP values were then normalized by dividing by the RFP signal at time  $t=0$  (which corresponds to the amount of IscA protein translated), which was measured using the above image analysis for RFP before magnetic exposure (magnetic fields did not affect RFP expression). All normalized values were then divided by the signal ratio at time  $t=0$  to yield a fold-change, which is now statistically useful because it can be applied across trials. Due to random variations around the plate (distance from magnet, high density, etc.), certain raw GFP fluorescent readings were magnitudes apart, so this method accounted for that. This also explains the relatively low fold-change values, since regions of high and low activity are averaged. A random sample of three microscope frames for each experiment were then averaged (standard deviation shown) to generate the following plots shown in Fig. 8.

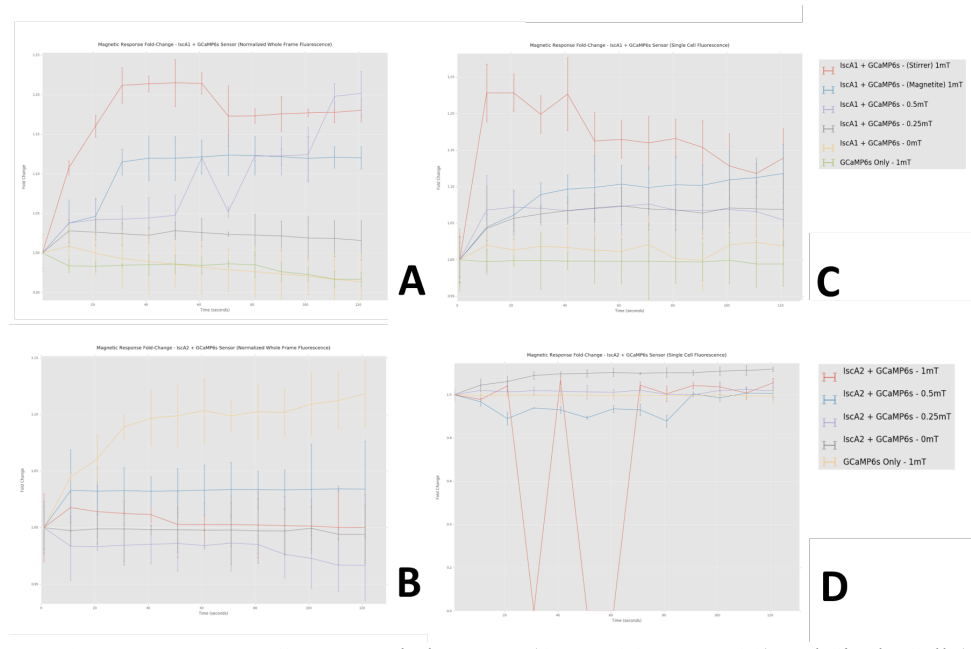


**Figure 8. Magnetic Response Fold Change:** Whole Frame (A - IscA1, B - IscA2) and Single Cell (C - IscA1, D - IscA2) plots in the previous figure were normalized by both RFP and fluorescent signal at t=0 to calculate the amount of fold-change. This process was repeated for both IscA1+GCaMP6s, IscA2 + GCaMP6s, and GCaMP6s across 0-1mT B-fields. Qualitatively, IscA1 (A, C) demonstrated binary control whereby the activation of B-fields stronger than 0.25mT generated calcium-induced fluorescence fold-changes. On the other hand, IscA2 (B, D) demonstrated little binary control (the zero-values in C represent a cell moving outside the field-of-view). Further statistical analysis was performed to quantitatively analyze binary control and the possibility of modular control. For each curve, we achieved a steady state fold-change by taking the average of fold-changes from 60 to 120s.

**Regression:** These steady-state values were then plotted to form a fold-change vs. B-field scatter plot for regression analysis (see appendix VI). For IscA1, there was a weak positive correlation formed from the data points ( $R=0.87$ ), while IscA2 shows no correlative signs of any modular control ( $R=0.36$ ). These signs indicate that our magnetogenetic sensor is not yet developed to the degree of modular control.

**T-Test:** However, the possibility of on/off control of our sensor in the presence of any magnetic field more substantial than Earth's background (ca.  $50\mu\text{T}$ ) seems likely even in this pilot stage. To test this statistically, we ran a t-test of the IscA1 + GCaMP6s co-transfected cells in 1mT fields against our positive and negative controls where we would expect no activity stimulated by magnetism. By combining variances to form two pooled means and standard deviations ( $n=12$ ), we found signal fold-change was  $1.14 \pm 0.06$  and  $0.98 \pm 0.05$ , yielding a p-value of 0.0009. Since  $p < 0.05$ , we have significant evidence to show that the fluorescent activation for this IscA1 based magnetic sensor is higher in the presence of 1.0mT fields than in the absence of one. We performed this test again at magnetic strengths of 0.5mT ( $1.13 \pm 0.04$ ,  $n=6$ ,  $p=0.0048$ ) and 0.25mT ( $1.04 \pm 0.04$ ,  $n=6$ ,  $p=0.0.1205$ ), and in our limited samples, we can see that the sensor is no longer statistically significant at magnetic strengths below 0.25mT, and we can only be confident that our sensor works at magnetic field strengths above 0.5mT.

However, we caution with this statistical result because the fold-change difference between experimental and control wells is only marginal due to various factors (human error, bleaching, etc.) that we cannot necessarily assert a substantial, causal mechanism that would be repeatably observable as a biological sensor. Still, our limited samples in this pilot does offer statistical evidence supporting a calcium-influx mechanism behind magnetoreception.

Furthermore, as an extension of our analysis, we could calculate the lower-limit sensitivity of our magnetic biosensor to be 0.25mT.

## Conclusion/Discussion

The results herein give rise to a genetic sensor based on cellular exposure to an external magnetic field. In our pilot study, we had three main conclusions - two of which corroborated the results in Long et al. 2015 on a smaller scale.<sup>6</sup> First, we were able to demonstrate the qualitative success of our IscA-sensor/calcium influx fluorescent reporter. While we have not confirmed the mechanism on a molecular level, we have no reason to believe that the iron-sulfur cluster assembly protein acting as a membrane-bound magnetoreceptor to promote calcium influx (as speculated in Long et al. 2015) is not true.<sup>6</sup> Future investigations must uncover the actual pathway mechanism. Still, this preliminary outcome contributes to the overall scientific discussion of magnetoreceptor-based mechanisms in which multiple chemical, magnetic induction, and magnetite-based hypotheses are being developed as potential mechanisms behind magnetoreception.<sup>9</sup>

Second, our data exhibits strong on-off control of IscA1 activating the calcium indicator in the presence of magnetic fields at a threshold above 0.25mT (and deactivation when the magnet is removed). This lower limit should be refined with more trials analyzed by stiffer experimental setup and more sophisticated image-analysis software to analyze our microscopy images. For example, our post-processing failed to account for z-axis movement of cells between frames (due to vibrations in our setup) that could make cells appear larger or smaller based on proximity to the microscope. While we simply used an average cell radius, better software can recalculate the actual change in radius between frames. A more stable experimental apparatus can reduce the amount of vibrations. But the possibility of binary control would become a powerful tool for biological control in targeted orthogonal gene regulation systems.

Lastly, unlike in Long et al. 2015, our constrained experiment could not establish modular control of this sensor of magnetic levels correlated to fluorescent activation. We concede that our sensor operates on low fold-changes subject to high variance. Additionally, some of our data could be confounded by environmental errors such as slight changes in lighting in the microscope room (we did our best to control these factors). More trials in more carefully controlled environments can address both these issues potentially allowing for us to establish modular control in the future. But our findings' statistical significance, corroborated by recent literature pursuing similar systems<sup>10</sup> posits a strong case supporting our magnetic biosensor.

We admit our project is still in the pilot phase. In a revamped design, we would attempt to link the constructs together and virally transfect the sensor plasmid to perfectly recreate Long et al. Other improvements include using mammalian antibiotic selection to purify our cells or designing IscA-specific antibodies for Western Blot analysis to check for proper synthesis of our iron-sulfur cluster assembly protein.

Future avenues of exploration remain: Do IscA1 gene homologues from other magnetic sensing organisms work more effectively? Does the magnetic biosensor work in other eukaryotic--and even prokaryotic--cells/organisms? On a cellular level, since the mechanism involves binding to the cellular cytoskeleton, does our mechanism extend to cells with different physical structures? Using different homologues and cell types can offer preliminary answers to these questions. On a broader scale, a further developed magnetogenetic system could be a powerful tool in synthetic biology, just like optogenetics was for neuromodulation. While our biosensor simply outputs fluorescence, by changing the genetic circuit, we can leverage already existing systems such as CRISPR-Cas9<sup>7</sup> or targeted drug therapies to maximize our sensor's utility. Uniquely, since our sensor is magnetically-activated, it can potentially access a wide-array of *non-invasive* therapies and treatments that are not possible with optogenetically-activated functions.<sup>11</sup>

## References

1. [Deisseroth Karl, et al. 2006. Next-Generation Optical Technologies for Illuminating Genetically Targeted Brain Circuits. The Journal of Neuroscience: the official journal of the Society for Neuroscience. 26.41: 10380.](#)
2. [Allen Brian, et al. 2015. Principles of Designing Interpretable Optogenetic Behavior Experiments. Learning & Memory. 22: 232-238.](#)
3. [Mora Cordula, et al. 2004. Magnetoreception and its trigeminal mediation in the homing pigeon. Nature. 432: 508-511.](#)
4. [Mandilaras Konstantinos, et al. 2012. Genes for iron metabolism influence circadian rhythms in \*Drosophila melanogaster\*. Metallomics. 4: 928-936.](#)
5. [Cozar-Castellano, et al. 2004. hlscA: a protein implicated in the biogenesis of iron-sulfur clusters. Biochim Biophys Acta. 1700\(2\): 179-88.](#)
6. [Long Xiaoyang, et al. 2015. Magnetogenetics: remote non-invasive magnetic activation of neuronal activity with a magnetoreceptor. Science Bulletin. 1-13.](#)
7. [Nihongaki Yuta, et al. 2015. Photoactivatable CRISPR-Cas9 for optogenetic genome editing. Nature Biotech. 33\(7\): 755-760.](#)
8. [Chen TW, et al. 2013. Ultrasensitive fluorescent proteins for imaging neuronal activity. Nature. 499: 295–300](#)
9. [Johnsen Sonke, 2000. The neurobiology of magnetoreception in vertebrate animals. Neuroscience. 23\(4\): 153-159.](#)
10. [Siying Qin, et al. 2015. A magnetic protein biocompass. Nature Materials. 1476: 4660.](#)
11. [John Horgan. 2013. Why “Optogenetic” Methods for Manipulating Brains Don’t Light Me Up.](#)

## Acknowledgements

The authors would like to personally thank Dr. Stanley Qi, Dr. Joseph Shih, Maddy Sides, Calvin Schmidt, Shireen Rudina, Cameron Kim, Tony Gao, the Stanley Qi Laboratory, and everyone in the Stanford Bioengineering Department for giving us these incredible opportunities in BIOE 44.

## **Appendix I. Biological Resources/Abbreviations**

1. pGP-CMV-GCaMP6s (s = slow) plasmid: <https://www.addgene.org/40753/>
2. pD669-AR Mammalian Transient Expression Vector Backbone from DNA 2.0: <https://www.dna20.com/eCommerce/catalog/datasheet/162>
3. IscA1 (Iron-Sulfur Cluster Assembly) Coding Sequence on iGEM Parts Registry: [http://parts.igem.org/Part:BBa\\_M36907](http://parts.igem.org/Part:BBa_M36907)
4. IscA2 (Iron-Sulfur Cluster Assembly) Coding Sequence on iGEM Parts Registry: [http://parts.igem.org/Part:BBa\\_M36908](http://parts.igem.org/Part:BBa_M36908)
5. IDT Codon Optimization for IscA Human Codon Optimization: <https://www.idtdna.com/CodonOpt>

## **Appendix II. Matlab Source Code for GFP Time-Lapse Image Analyzer**

```
%{  
Written by: Sreyas Misra November 23, 2015  
Bioengineering 44 Group: MTS Checkplus  
Tested using Matlab R2014a  
  
%%%%%%%%%%%%%  
% This script analyzes GFP changes in time-lapse microscope videos.  
%}  
  
v = VideoReader('1mT_IscA1_Timelapse.avi'); % Substitute for respective video file  
% Reads in 1MT video timelapse by creating VR object  
  
frames = read(v,[1,Inf]);  
% Reads all the frames in the video  
  
[row,col,color,num] = size(frames);  
% Get dimensions  
  
images = [];  
normFluo = [];  
singCell = [];  
  
radius = 40;  
% Cell radius %  
  
interval = 10;  
% length of time interval between frames %  
  
for i = 1:num  
  
    I = frames(:,:,:,:i);  
    I = rgb2gray(I);  
  
    % Make Gaussian filter (width = 3*sigma to remove discontinuities). %  
  
    G = fspecial('gaussian',[15 15],5);  
    I = imfilter(I,G,'same');  
  
    % Use Otsu's Method to Find Threshold %  
  
    level = graythresh(I);  
    threshold = double(((max(max(I)) - min(min(I)))*level + min(min(I))));  
    BW1 = roicolor(I,threshold,max(max(I)));  
    BW2 = roicolor(I,min(min(I)),threshold);  
    Areal = sum(I(BW1))/sum(sum(BW1));
```

```

Area2 = sum(I(BW2))/sum(sum(BW2));
threshold = (Areal - Area2)/2 + Area2;

% Apply Threshold to Image to floor sub-threshold pixels %

for rw = 1:1:row
for cl = 1:1:col
    if I(rw,cl) <= threshold
        I(rw,cl) = 0;
    end
end
end
% total normalized fluorescence %%%%%%%%
[r,c] = find(I > 0);

normFluo = [normFluo, sum(sum(I))/length(r)];
%%%%%%%%%%%%%%%
%%%%% 1-cell fluorescence - pick hotspot cell %%

% Find hotspot cell range %

[x, y] = find(I == max(max(I)));

sumFluo = 0;

% +/- cells radius at x and y centers %
for j = (round(mean(x))-radius):(round(mean(x))+radius)
for k = (round(mean(y))-radius):(round(mean(y))+radius)

    sumFluo = I(j,k) + sumFluo;
end
end

singCell = [singCell, sum(sum(I((round(mean(x))-radius): ...
(round(mean(x))+radius),(round(mean(y))-radius): ...
(round(mean(y))+radius))))/(radius^2)];

%%%%%%%%%%%%%%%
end

t = 1:interval:num*interval;
% Update parameters as appropriate for each video
plot(t,normFluo)
title('1MT - Normalized Fluorescence for Time-Lapse Microscope FOV')
xlabel('Time (seconds)')
ylabel('Grayscale Fluorescence Intensity')
figure(2)
plot(t,singCell)
title('1MT - Fluorescence of a single cell')
xlabel('Time (seconds)')
ylabel('Grayscale Fluorescence Intensity')

```

### Appendix III. Matlab Source Code for GFP Still Image Analyzer

```

%{
Written by: Sreyas Misra November 23, 2015
Adapted by: Michael Becich December 1, 2015
Bioengineering 44 Group: MTS Checkplus
Tested using Matlab R2015b
%%%%%%%%%%%%%%%
%%%%%%%%%%%%%%%

```

```

This script analyzes GFP levels in microscope still images.
%}

files = dir('*.png');
for file = files'
    file.name
    I = imread(file.name);
    % Do some stuff

    %initialize arrays
    images = [];
    normFluo = [];
    singCell = [];

    radius = 40;
    % Cell radius %

    interval = 10;
    % length of time interval between frames %

    [row,col,color] = size(I);
    num=1;
    I = rgb2gray(I);

    % Make Gaussian filter (width = 3*sigma to remove discontinuities). %

    G = fspecial('gaussian',[15 15],5);
    I = imfilter(I,G,'same');

    % Use Otsu's Method to Find Threshold %

    level = graythresh(I);
    threshold = double(((max(max(I)) - min(min(I)))*level + min(min(I))));
    BW1 = roicolor(I,threshold,max(max(I)));
    BW2 = roicolor(I,min(min(I)),threshold);
    Area1 = sum(I(BW1))/sum(sum(BW1));
    Area2 = sum(I(BW2))/sum(sum(BW2));
    threshold = (Area1 - Area2)/2 + Area2;

    % Apply Threshold to Image to floor sub-threshold pixels %

    for rw = 1:1:row
        for cl = 1:1:col
            if I(rw,cl) <= threshold
                I(rw,cl) = 0;
            end
        end
    end
    % total normalized fluorescence %%%%%%%%
    [r,c] = find(I > 0);

    normFluo = [normFluo, sum(sum(I))/length(r)]
    %%%%%%%%%%%%%%%%
    % 1-cell fluorescence - pick hotspot cell %%
    % Find hotspot cell range %

    [x, y] = find(I == max(max(I)));

    sumFluo = 0;

    % +/- cells radius at x and y centers %
    %      if(radius > mean(x))

```

```

%
% radius=round(mean(x))-1;
%
% end;
%
% if(radius > mean(y))
%
% radius=round(mean(y))-1;
%
% end;
for j = (round(mean(x))-radius):(round(mean(x))+radius)
for k = (round(mean(y))-radius):(round(mean(y))+radius)

    sumFluo = I(j,k) + sumFluo;
end
end

singCell = [singCell, sum(sum(I((round(mean(x))-radius): ...
(round(mean(x))+radius),(round(mean(y))-radius): ...
(round(mean(y))+radius))))/(radius^2)]
%%%%%%%%%%%%%%%
end

```

#### **Appendix IV. Example of Image Analysis Techniques**

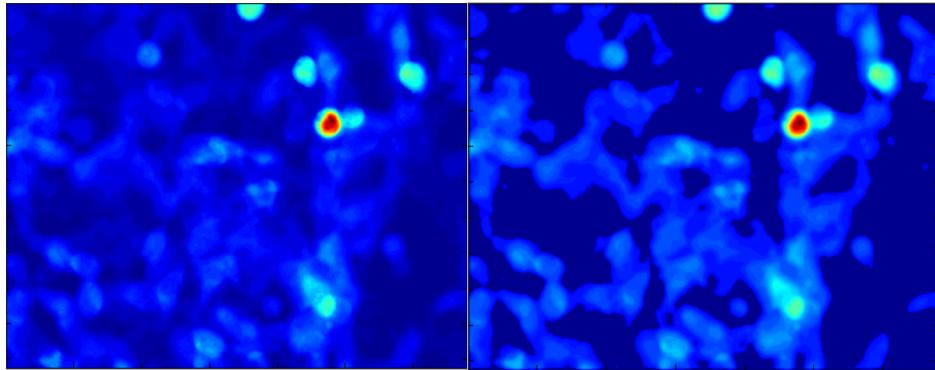


Image post-processing of our fluorescence images (shown on right) significantly reduced the amount of non-fluorescing objects such that a greater proportion of the image comprised high-fluorescence cells (as compared to the left).

#### **Appendix V.**

Video of magnetogenetic control when B-field of 2.0mT was applied at 0 seconds and removed at 60 seconds:

<http://thomaskenyinglau.com/isca1fluctuating.mp4>

#### **Appendix VI. Magnetic Modular Control Regression Plot**

